Editors' Suggestion

Selective Solvent-Induced Stabilization of Polar Oxide Surfaces in an Electrochemical Environment

Su-Hyun Yoo, Mira Todorova,* and Jörg Neugebauer
Department of Computational Materials Design, Max-Planck-Institut für Eisenforschung GmbH, Max-Planck-Str. 1, D-40237 Düsseldorf, Germany

(Received 17 October 2017; revised manuscript received 10 December 2017; published 7 February 2018)

The impact of an electrochemical environment on the thermodynamic stability of polar oxide surfaces is investigated for the example of ZnO(0001) surfaces immersed in water using density functional theory calculations. We show that solvation effects are highly selective: They have little effect on surfaces showing a metallic character, but largely stabilize semiconducting structures, particularly those that have a high electrostatic penalty in vacuum. The high selectivity is shown to have direct consequences for the surface phase diagram and explains, e.g., why certain surface structures could be observed only in an electrochemical environment.

DOI: 10.1103/PhysRevLett.120.066101

Solid-liquid interfaces are at the heart of many problems of practical importance, such as water electrolysis and batteries, photo catalytic water splitting, electrocatalysis, or corrosion. Understanding what surface structures form when the solid is immersed in an aqueous electrolyte is, therefore, of particularly high interest. In contrast to its importance, we presently know little about the role the electrolyte plays in the stabilization of such structures. There is consensus that dissociated water fragments such as H^+ or OH^- form strong chemical bonds with the surface and these adsorption mechanisms are generally included in the respective *ab initio* calculations [1–3]. Including effects caused by the polarization and electrostatic screening of the electrolyte are less straightforward to implement and their treatment varies. The three main conceptual approaches have been all applied to the study of metal-water interfaces: (i) explicit water *ab initio* molecular dynamics simulations [1], which is the most accurate but also most expensive approach, (ii) surface science setup of a slab (with adsorbates) in vacuum where solvation effects are included *a posteriori* via a thermodynamic treatment [2,4], and (iii) use of an implicit solvent [5], which describes the solvent as a polarizable continuum reflecting the screening properties of water [6–10] and constitutes a compromise between the two aforementioned cases. Approach (ii) has been occasionally used to study oxides [11] and has been recently extended by adding a few water layers in addition to the specifically adsorbed species at the interface [12,13]. The general picture is that the impact of the solvent, next to explicit chemisorption of H or OH, is small [13].

In the present work, we show that when going from metal to semiconducting surfaces solvation effects become important: They generally lower the surface energy (making these surfaces more stable) and are highly selective—surfaces with a high electrostatic penalty or a stronger semiconducting character gain substantially more energy.

We focus on ZnO(0001) surfaces as a prototypical example of a polar oxide surface. Zinc oxide itself is of interest for a wide range of applications ranging from catalysis, corrosion, gas sensing, to opto- and microelectronics [14–20]. It is a wide band gap semiconductor, which crystallizes in the wurtzite structure. Cleavage of ZnO perpendicular to the c axis leads to the formation of a zinc terminated (0001) and an oxygen terminated $(000\bar{1})$ polar surface. At the unreconstructed surface, each Zn(O) dangling bond at the $\mathrm{ZnO}(0001)[\mathrm{ZnO}(000\bar{1})]$ surface is partially filled and contains $1/2$ $(3/2)$ electrons rendering these surfaces metallic. Removing the ensuing surface charge is the driving force triggering reconstructions. The reconstructions strive to minimize the electronic energy [commonly formulated as the electron counting (EC) rule [21]: all energetically low-lying anion dangling bond states are doubly occupied, all cation dangling bond states are empty] and the electrostatic energy (by optimizing the arrangement of the charged surface atoms).

To access how solvation affects the stabilization of surface phases we use density functional theory (DFT) calculated energies [22–30] to construct surface Pourbaix diagrams [2] for ZnO(0001). Pourbaix diagrams reveal the thermodynamically stable phases in dependence of the relevant environmental conditions of pH and electrode potential U. Traditionally they are constructed for bulk phases and as such reveal conditions for which different ions or solid bulk phases associated with a given system are stable. Surface Pourbaix diagrams show, in contrast, which surface structures are thermodynamically stable for conditions of pH and U. To construct a surface Pourbaix diagram for ZnO we perform for each considered ZnO(0001) surface structure one calculation for the surface

in vacuum and another calculation for the surface in contact with an implicit solvent. Because implicit solvation models do not account for explicit chemical interactions of the solute with the environment, we include in the pool of possible surface reconstructions structures that contain chemically reactive water constituents, such as OH^- or H^+ ions. Thus, effects such as adsorption of these ions are included. However, the energetically much smaller effects due to hydrogen bonding between the solute and the solvent are neglected. Also, the shape function of the cavity encompassing the solute and related cavitation and dispersion terms are determined by a fit to solvation energies of a set of small molecules [10,31,32], rather than surfaces. We use the implicit solvation model VASPsol, implemented in VASP by Mathew *et al.* [32]. This model assumes a diffuse dielectric cavity: the solvent-accessible surface is determined from the quantum mechanically calculated electronic charge density of the solute and the dielectric constant of the implicit solvent is smoothly varied at the interface until it reaches its full value of $\varepsilon = 80$ (the dielectric constant of water). Dipole corrections [33] are used for the calculations of slab in vacuum, but not for calculations with solvent [34].

Based on insights gained in previous studies [29,30,35,36] we focus on about 50 low energy surface configurations as the most likely candidates for stable surface phases at polar Zn terminated ZnO(0001) surfaces. We use surface cells of up to $(\sqrt{48}\times\sqrt{48})$ times the size of the surface unit cell and consider configurations including the pristine surface, vacancy structures, triangular reconstructions, and adsorbate structures on both the pristine and the reconstructed surfaces. Triangular structures of side length n are constructed by removing $n(n+1)/2$ Zn atoms and $n(n-1)/2$ O atoms from the surface bilayer. A (2×2) Zn-vacancy reconstruction can be considered as the smallest triangular phase (i.e., $n1$) and an example of the $n7$ triangular reconstruction is seen in the 5th panel of Fig. 1(c). To account for the possibility that triangular reconstructions can penetrate deeper into the surface [35,37], we considered also double triangles. In the double triangles $n6n3$ and $n7n3$ a second inverted triangle (here of side length 3) is created by removing atoms from the second layer within the boundaries of the first layer triangle [e.g., panels 6 and 7 in Fig. 1(c)]. Triangles penetrating the surface beyond the second ZnO bilayer were not considered, but we cannot exclude the possibility of their existence. Depending on the size of the used surface unit cell, the triangular structures may or may not fulfill electron counting. For example, in a $(\sqrt{12}\times\sqrt{12})$ surface cell the number of O and Zn partially filled dangling bonds is balanced for a $n3$-triangular reconstruction, and we term this reconstruction $n3$ (EC). The same is not true if the $n3$ triangular structure is created in a $(\sqrt{48}\times\sqrt{48})$ surface cell, in which case there is an excess of partially filled Zn-dangling bonds at the surface. We annotate the respective triangular reconstruction as $n3$. The biggest EC triangular reconstruction we were able to perform a converged calculation for was $n4$. For the double triangles we were able to achieve electron counting structures only following adsorption of OH and H species. However, in view of the easy availability of OH and H species through the aqueous environment, it is more than

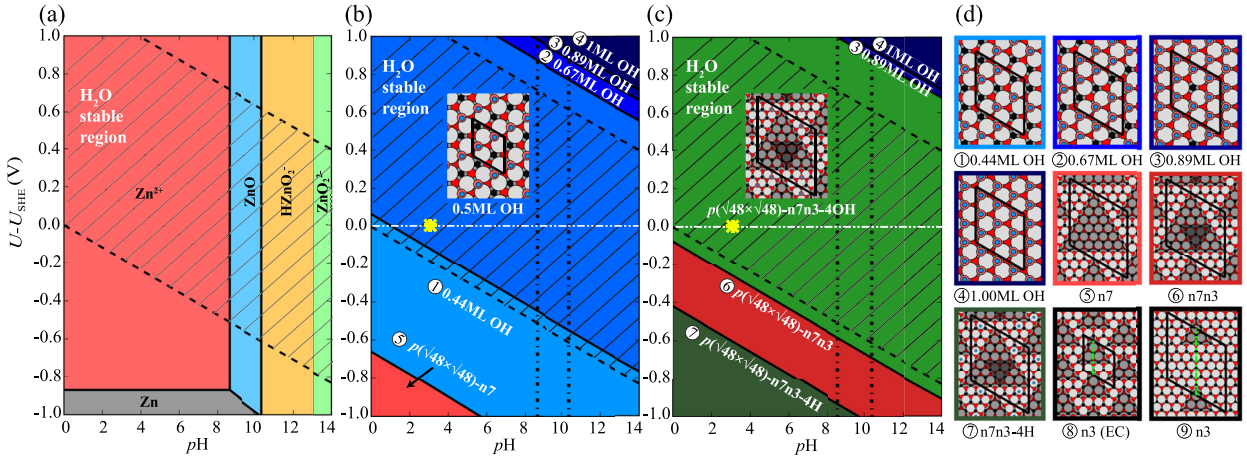

FIG. 1. Pourbaix diagrams, showing the stability of Zn phases as a function of the solution's pH and the electrode potential U referenced to the standard hydrogen electrode potential U_{SHE}. (a) Pourbaix diagram for zinc, adapted from Ref. [38]. (b) and (c) Surface Pourbaix diagrams for the ZnO(0001)-Zn surface constructed using energies obtained from DFT calculations (b) without and (c) with a solvent. Colors are used to discriminate the different surface phases: structures with adsorbates on the smooth bulk terminated surface (blue), triangular reconstructions (red), adsorbate-passivated triangular reconstructions (green). The black hashed area shows the water stability region (see text). The stability region of bulk ZnO is superimposed onto the surface diagrams (vertical black dotted lines). The yellow star marks the experimental condition at which triangular reconstructions have been observed at the surface in an *in situ* AFM study [37]. (d) Top view of the stable surface phases found within the phase diagram. Zn, O, and H atoms are shown as white, red, and blue balls, respectively. The colors used for the frames correspond to the colors used in the surface Pourbaix diagrams.

likely that unsaturated partially filled, and thus reactive, dangling bonds will attract adsorbates. Finally, we also consider OH adsorbate structures on the bulk terminated ZnO(0001)-Zn surface for coverages between 0.11 and 1.00 ML, as well as mixed OH and O structures, and O adsorbate structures.

The calculated DFT energies are used to assess the thermodynamic stability of the investigated ZnO(0001)-Zn surface structures by evaluating the excess Gibbs free surface energy, ΔG^{α}. Since the surface is a thermodynamically open system we get

$$\Delta G^{\alpha} = (E^{\alpha}_{\mathrm{tot}} - E^{\mathrm{clean}}_{\mathrm{tot}}) - \sum N_i \mu_i. \quad (1)$$

This energy is thus the DFT total energy $E^{\alpha}_{\mathrm{tot}}$ of a surface structure α referenced to the energies of the pristine surface $E^{\mathrm{clean}}_{\mathrm{tot}}$ and the reservoirs μ_i of elements i, of which N_i species are exchanged with the environment. We note that the DFT total energy obtained in the presence of the solvent contains the penalty contributions due to the cavitation and polarization of water [32]. Cavitation becomes important for example for corrugated surface reconstructions, where the interface area is increased compared to a flat surface. Surface vibration entropy contributions, which are key to understanding the stabilization of ZnO(0001)-Zn surfaces in a gas phase environment [30], were found to be small for temperatures relevant for wet electrochemistry ($T \approx 300$ K) and are not included [39]. To compute the surface Pourbaix diagram we express the chemical potential as a function of pH and U. Thereto we utilize our grand-canonical approach extending methodologies widely used to study point defects in semiconductors [40,41] to the description of stability and concentration of ions in liquids [38]. As shown there, the hydrogen chemical potential is a function of pH and U:

$$\mu_{\mathrm{H}}(p\mathrm{H}, U) = e(U - U_{\mathrm{SHE}}) - k_B T \ln 10 \; p\mathrm{H}. \quad (2)$$

Here U_{SHE} denotes the reference potential of the standard hydrogen electrode.

The thermodynamic bounds in which the chemical potentials can be varied are determined by other phases becoming thermodynamically more stable. We follow the conventional approach and reference the chemical potentials to their respective elemental phase (here H_2 gas, O_2 gas, and Zn bulk). As will be shown later this does not actually mean that the potential can also reach these values: In an electrolyte more restrictive boundaries exist to enforce the stability of the electrolyte or the bulk system. Specifically, immersing ZnO in water represents a two-phase coexistence region in the Zn, O, H phase diagram. In terms of chemical potentials, this can be expressed by enforcing thermodynamic stability both with respect to water and ZnO:

$$\mu_{\mathrm{O}} = \Delta_f G[\mathrm{H_2O}] - 2\mu_{\mathrm{H}} \quad (3)$$

$$\mu_{\mathrm{Zn}} = \Delta_f G[\mathrm{ZnO}] - \mu_{\mathrm{O}}(\mu_{\mathrm{H}}). \quad (4)$$

Thus, while the system is characterized by three chemical potentials (Zn, O, H), the fact that both water and ZnO coexist reduces the thermodynamic degrees of freedom resulting in only a single chemical potential that can be chosen freely. We choose μ_{H} as expressed in Eq. (2) so that all chemical potentials can be expressed by the electrochemical conditions pH and U.

The fact that we have only a single degree of freedom in the chemical potentials is also reflected in the surface Pourbaix diagrams [Figs. 1(b) and 1(c)] where all phase boundaries are parallel to each other. The stability region of water, shown as a hashed area between two dashed black lines, shows conditions under which water is stable against H_2 or O_2 formation.

Constructing a bulk Pourbaix diagram for zinc [42] [Fig. 1(a)] requires the consideration of zinc chemical potentials beyond the ZnO stability range. In this case μ_{Zn} is no longer uniquely expressed by μ_{O} and one needs to consider the variation of two independent chemical potentials, i.e., $\mu_{\mathrm{O}}(\mu_{\mathrm{H}})$ [or equivalently $\mu_{\mathrm{H}}(\mu_{\mathrm{O}})$] and μ_{Zn} [38]. In this case, it is no longer compulsory for phase transition lines to be parallel to the water stability lines, as seen in the Pourbaix diagram for Zn shown in Fig. 1(a).

To study how the solvent affects surface stability and selectivity we consider the following two cases: without a solvent [Fig. 1(b)] and with a solvent [Fig. 1(c)]. Comparing the phase diagram with and without a solvent provides direct insight as to whether the solvent is selective, i.e., whether it stabilizes or destabilizes certain phases. For a solvent, which shows no selectivity, the two surface Pourbaix diagrams would be identical. As can be seen in Fig. 1 the impact of the solvent is dramatic: It leads not only to a shift of the phase boundaries (which would indicate that one surface profits energetically more than the other), but also to the stabilization of surface reconstructions that are thermodynamically unstable in an ambient gas phase environment. Water thus turns out to be surprisingly selective allowing the formation of structures that are thermodynamically unstable under normal conditions. The left diagram [Fig. 1(b)], in which the effect of solvation is reduced to the chemisorption of the dissociated water fragments H and OH, is dominated by structures with adsorbates on the bulk terminated surface (blue colors). The right diagram [Fig. 1(c)] is dominated by triangular reconstructions (red and green colors). It is noteworthy that only the right diagram [Fig. 1(c)], constructed from DFT energy calculations with explicitly included solvation effects, is able to account for the experimental observation of triangular phases. These are seen in *in situ* AFM experiments by Valtiner *et al.* [37] at open circuit potential conditions ($U - U_{\mathrm{SHE}} = 0$ V) and $p\mathrm{H} \approx 3$ (marked by a yellow star).

In thermodynamic equilibrium, the chemical potentials at the surface and in the bulk are identical allowing us to superimpose the bulk and surface Pourbaix diagrams in

Fig. 1. As shown in Fig. 1(a) the region where bulk ZnO is stable is limited to a rather narrow interval of pH values between 8.6 and 10.4. Plotting these boundaries in the surface Pourbaix diagrams [Figs. 1(b) and 1(c)] shows that the experimental conditions reported by Valtiner *et al.* [37] are actually significantly away from the thermodynamic bulk stability region. It also indicates that at nonequilibrium conditions, which are common in electrochemistry, the surface Pourbaix diagram is not restricted to the rather small region where the ZnO bulk is stable. The reason is that the kinetic mechanisms, which bring surfaces to thermodynamic equilibrium, are much faster than bulk kinetics.

To understand why the triangular structures profit more from the electrolyte than the other surface structures we evaluate their solvation energy, E_{solv}. This quantity is the energy difference between the DFT total energy of the system in vacuum and the system in contact with the solvent. Figure 2(a) shows the dependence of the solvation energy on the amount of unpaired electrons at the surface [43], which is a measure of metallicity and its deviation from charge neutrality. As can be seen, the solvation energy decreases with increasing metallicity; i.e., the energy the system gains by solvation increases. Solvation thus strongly favors nonmetallic surfaces over the ones with metallic character.

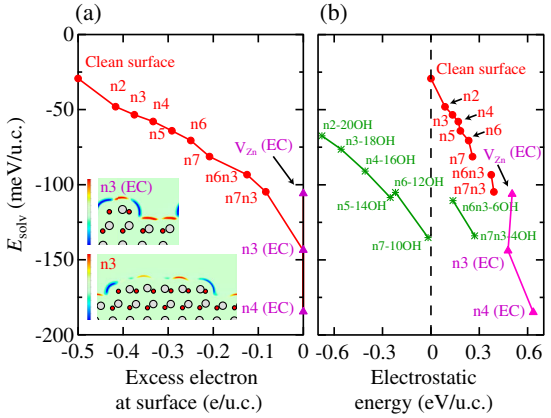

FIG. 2. Solvation energies of ZnO(0001)-Zn surface structures plotted as a function of (a) the excess electrons at the surface and (b) the electrostatic energy of surface phases referenced to that of the clean surface. The excess electrons at the surface correspond to the number of unsaturated electrons in the partially filled surface Zn dangling bonds per unit cell (see text). The colors identify triangular phases for which the electron counting rule (EC) is not fulfilled (red), fulfilled purely by a triangular reconstruction (purple), and fulfilled due to the presence of hydroxyl adsorbates in addition to the triangular reconstruction (green). EC obeying surface phases (i.e., purple and green) are charge neutral [21]. Inset in (a) are electron difference density plots depicting the screening charge at the interface [blue, electron accumulation ($\min \approx -10^{-4}\ e^-/\mathrm{Bohr}^3$); red, electron depletion ($\max \approx 10^{-4}\ e^-/\mathrm{Bohr}^3$)] perpendicular to the interface and along the direction indicated by dashed green lines in Fig. 1(d).

The increased screening and the strong selectivity towards nonmetallic surface structures, which leads to the solvation energy gain with decreasing metallicity (screening) seen in Fig. 2(a), can be understood as follows: Metallic surfaces have a much higher intrinsic electronic polarizability compared to semiconductor surfaces and are thus able to efficiently screen electrostatic charges. For surfaces obeying electron counting, i.e., which are semiconducting and thus lack efficient electrostatic screening, the solvent provides almost metallic screening (the dielectric constant of water is 80) and thus reduces electrostatic penalties at the surface. If screening is already an intrinsic part of the surface (i.e., for surfaces having excess electron or holes) additional screening brings no extra energy gain. This is seen in the difference electron density plot shown as insets in Fig. 2(a). For the exemplarily chosen $n3$ (EC) structure the screening charge at the interface forms a tight envelope of regions with electron accumulation (blue) and depletion (red) electrostatically shielding the ZnO surface atoms. In the case of the metallic (non EC) $n3$ reconstruction the screening charge is much more diffuse and 3 times lower compared to the EC case.

Figure 2(b) shows a further correlation between solvation energy and surface structures. As can be seen, surfaces with a high electrostatic penalty profit more from solvation than structures with low penalty. The origin of this behavior relates to the preceding screening discussion: The higher the electrostatic penalty the more energy can be gained by screening. The presence of this mechanism stabilizes triangular structures [e.g., structures 5–9 in Fig. 1(d)], while nontriangular structures profit to a lesser extent. The reason is the high electrostatic penalty in the triangular structures, which is a direct consequence of the large separation between negative charges at the edges (filled O dangling bonds) and positive charges inside the triangle (empty Zn dangling bonds). The correlations identified in this study reveal that the solvation energy is highly discriminating and key to understand and eventually control the appearance and thermodynamic stability of structures at semiconducting surfaces.

Next to the selectivity discussed above, the solvation energies shown in Fig. 2 have also another remarkable feature. They are all negative (exothermic), implying that wetting is expected for all studied surfaces. Furthermore, an exothermic solvation energy implies that a solvated surface has a lower energy and can be thus formed easier. As pointed out by Griffith [44], this can lead to enhanced embrittlement, since the energy needed to create cracks is reduced. This insight makes our observations also important for areas like geology. There it has been suggested that enhanced crack growth in the presence of water and electrolytes is related to a surface energy reduction [45]. Furthermore, observations suggest that electrostatic interactions with the environment, as well as its screening properties, are very important [46,47].

In conclusion, by studying ZnO(0001) as a prototype oxide surface immersed in water we show that solvation effects are substantial and highly selective. Solvation effects are small on surfaces with metallic character since energetically unfavorable electrostatic interactions can be efficiently screened by the surface itself. However, solvation strongly favors surface reconstructions with semiconducting character, where surface screening alone is not very efficient. In particular, reconstructions, which have in vacuum a high electrostatic penalty, profit from stabilization. Electrochemical conditions thus allow us to realize surface reconstructions that are thermodynamically forbidden in vacuum. These concepts are general and apply to other semiconductor-oxide surfaces. As such, they provide new insight into the enhanced crack formation in humid environments discussed in geology [45,46] and may be used to provide synthesis routes for designing surfaces with, e.g., controllable or improved catalytic properties.

This work is supported by the Cluster of Excellence RESOLV (EXC 1069) funded by the Deutsche Forschungsgemeinschaft.

*Corresponding author.
m.todorova@mpie.de

[1] C. Taylor, R. Kelly, and M. Neurock, First-principles calculations of the electrochemical reactions of water at an immersed $Ni(111)/H_2O$ interface, J. Electrochem. Soc. **153**, E207 (2006).
[2] H. Hansen, J. Rossmeisl, and J. Norskov, Surface pourbaix diagrams and oxygen reduction activity of Pt, Ag and Ni(111) surfaces studied by DFT, Phys. Chem. Chem. Phys. **10**, 3722 (2008).
[3] S. Schnur and A. Groß, Challenges in the first-principles description of reactions in electrocatalysis, Catal. Today **165**, 129 (2011).
[4] L. Tang, B. Han, K. Persson, C. Friesen, T. He, K. Sieradzki, and G. Ceder, Electrochemical stability of nanometer-scale Pt particles in acidic environments, J. Am. Chem. Soc. **132**, 596 (2010).
[5] K. Williams, J. Labukas, V. Rodriguez-Santiago, and J. Andzelm, First principles modeling of water dissociation on Mg(0001) and development of a Mg surface pourbaix diagram, Corrosion (Houston) **71**, 209 (2015).
[6] H. M. Senn, P. M. Margl, R. Schmid, T. Ziegler, and P. E. Blöchl, Ab initio molecular dynamics with a continuum solvation model, J. Chem. Phys. **118**, 1089 (2003).
[7] J. Fattenbert and F. Gygi, Density functional theory for efficient ab initio molecular dynamics simulations in solution, J. Comput. Chem. **23**, 662 (2002).
[8] J. Fattenbert and F. Gygi, First-principles molecular dynamics simulations in a continuum solvent, Int. J. Quantum Chem. **93**, 139 (2003).
[9] D. A. Scherlis, J.-L. Fattebert, F. Gygi, M. Cococcioni, and N. Marzari, A unified electrostatic and cavitation model for first-principles molecular dynamics in solution, J. Chem. Phys. **124**, 074103 (2006).
[10] O. Andreussi, I. Dabo, and N. Marzari, Revised self-consistent continuum solvation in electronic-structure calculations, J. Chem. Phys. **136**, 064102 (2012).
[11] H. Hansen, I. Man, F. Studt, F. Abild-Pedersen, T. Bligaard, and J. Rossmeisl, Electrochemical chlorine evolution at rutile oxide (110) surfaces, Phys. Chem. Chem. Phys. **12**, 283 (2010).
[12] E. Watanabe, J. Rossmeisl, M. Björketun, H. Ushiyama, and K. Yamashita, Atomic-scale analysis of the RuO_2/water interface under electrochemical conditions, J. Phys. Chem. C **120**, 8096 (2016).
[13] S. Sakong, M. Naderian, K. Mathew, R. G. Hennig, and A. Groß, Density functional theory study of the electrochemical interface between a Pt electrode and an aqueous electrolyte using an implicit solvent method, J. Chem. Phys. **142**, 234107 (2015).
[14] C. Wöll, The chemistry and physics of zinc oxide surfaces, Prog. Surf. Sci. **82**, 55 (2007).
[15] M. Kurtz, J. Strunk, O. Hinrichsen, M. Muhler, K. Fink, B. Meyer, and C. Wöll, Active sites on oxide surfaces: ZnO-catalyzed synthesis of methanol from CO and H_2, Angew. Chem., Intl. Ed. **44**, 2790 (2005).
[16] A. B. Djurisic, X. Chen, Y. H. Leung, and A. M. C. Ng, ZnO nanostructures: growth, properties and applications, J. Mater. Chem. **22**, 6526 (2012).
[17] A. Mclaren, T. Valdes-Solis, G. Li, and S. C. Tsang, Shape and size effects of ZnO nanocrystals on photocatalytic activity, J. Am. Chem. Soc. **131**, 12540 (2009).
[18] A. Janotti and C. G. Van de Walle, Fundamentals of zinc oxide as a semiconductor, Rep. Prog. Phys. **72**, 126501 (2009).
[19] J. E. Northrup and J. Neugebauer, Metal-adlayer-stabilized ZnO(0001) surfaces: Toward a new growth mode for oxides, Appl. Phys. Lett. **87**, 141914 (2005).
[20] B. Meyer and D. Marx, Density-functional study of the structure and stability of ZnO surfaces, Phys. Rev. B **67**, 035403 (2003).
[21] M. D. Pashley, Electron counting model and its application to island structures on molecular-beam epitaxy grown GaAs(001) and ZnSe(001), Phys. Rev. B **40**, 10481 (1989).
[22] See the Supplemental Material at http://link.aps.org/supplemental/10.1103/PhysRevLett.120.066101, which includes Refs. [23–30] for the computational details.
[23] J. P. Perdew, K. Burke, and M. Ernzerhof, Generalized Gradient Approximation Made Simple, Phys. Rev. Lett. **77**, 3865 (1996).
[24] P. E. Blöchl, Projector augmented-wave method, Phys. Rev. B **50**, 17953 (1994).
[25] G. Kresse and J. Furthmüller, Efficient iterative schemes for ab initio total-energy calculations using a plane-wave basis set, Phys. Rev. B **54**, 11169 (1996).
[26] G. Kresse and J. Furthmüller, Efficiency of ab-initio total energy calculations for metals and semiconductors using a plane-wave basis set, Comput. Mater. Sci. **6**, 15 (1996).
[27] H. Karzel *et al.*, Lattice dynamics and hyperfine interactions in ZnO and ZnSe at high external pressures, Phys. Rev. B **53**, 11425 (1996).
[28] S. Desgreniers, High-density phases of ZnO: Structural and compressive parameters, Phys. Rev. B **58**, 14102 (1998).

[29] O. Dulub, U. Diebold, and G. Kresse, Novel Stabilization Mechanism on Polar Surfaces: ZnO(0001)-Zn, Phys. Rev. Lett. **90**, 016102 (2003).

[30] M. Valtiner, M. Todorova, G. Grundmeier, and J. Neugebauer, Temperature Stabilized Surface Reconstructions at Polar ZnO(0001), Phys. Rev. Lett. **103**, 065502 (2009).

[31] D. Gunceler, K. Letchworth-Weaver, R. Sundararaman, K. Schwarz, and T. A. Arias, The importance of nonlinear fluid response in joint density-functional theory studies of battery systems, Model. Simul. Mater. Sci. Eng. **21**, 074005 (2013).

[32] K. Mathew, R. Sundararaman, K. Letchworth-Weaver, T. A. Arias, and R. G. Hennig, Implicit solvation model for density-functional study of nanocrystal surfaces and reaction pathways, J. Chem. Phys. **140**, 084106 (2014).

[33] J. Neugebauer and M. Scheffler, Adsorbate-substrate and adsorbate-adsorbate interactions of Na and K adlayers on Al(111), Phys. Rev. B **46**, 16067 (1992).

[34] See Supplemental Material at http://link.aps.org/supplemental/10.1103/PhysRevLett.120.066101 for dipole correction.

[35] G. Kresse, O. Dulub, and U. Diebold, Competing stabilization mechanism for the polar ZnO(0001)-Zn surface, Phys. Rev. B **68**, 245409 (2003).

[36] M. Valtiner, M. Todorova, and J. Neugebauer, Hydrogen adsorption on polar ZnO(0001)-Zn: Extending equilibrium surface phase diagrams to kinetically stabilized structures, Phys. Rev. B **82**, 165418 (2010).

[37] M. Valtiner, S. Borodin, and G. Grundmeier, Stabilization and acidic dissolution mechanism of single-crystalline ZnO(0001) surfaces in electrolytes studied by in-situ AFM imaging and ex-situ LEED, Langmuir **24**, 5350 (2008).

[38] M. Todorova and J. Neugebauer, Extending the concept of defect chemistry from semiconductor physics to electrochemistry, Phys. Rev. Applied **1**, 014001 (2014).

[39] We carefully checked that surface vibrational entropy contributions to the energy are small (for details see the Supplemental Material [34]) and safe to neglect in the present study.

[40] C. G. Van de Walle and J. Neugebauer, First-principles calculations for defects and impurities: Applications to III-nitrides, J. Appl. Phys. **95**, 3851 (2004).

[41] C. Freysoldt, B. Grabowski, T. Hickel, J. Neugebauer, G. Kresse, A. Janotti, and C. G. Van de Walle, First-principles calculations for point defects in solids, Rev. Mod. Phys. **86**, 253 (2014).

[42] The Pourbaix diagram for Zn bulk was constructed following the procedure described in Ref. [38] using tabulated thermodynamic data for the solvation energies of the considered ions.

[43] The number of excess electrons is calculated as $[0.5(n_{\mathrm{O}} - n_{\mathrm{Zn}})/(\text{size of unit cell})]$, where n_{O} (n_{Zn}) is the number of partially filled O(Zn) dangling bonds at the surface, assuming O(Zn) dangling bonds at the surface are partially filled with $3/2$ $(1/2)$ electrons.

[44] A. Griffith, VI. the phenomena of rupture and flow in solids, Phil. Trans. R. Soc. A **221**, 163 (1921).

[45] G. Parks, Surface and interfacial free energies of quartz, J. Geophys. Res. Solid Earth **89**, 3997 (1984).

[46] S. Freiman, Effects of chemical environments on slow crack growth in glasses and ceramics, J. Geophys. Res. Solid Earth **89**, 4072 (1984).

[47] J. Card, R. Cannon, E. Saiz, A. Tomsia, and R. Ritchie, On the physics of moisture-induced cracking in metal-glass (copper-silica) interfaces, J. Appl. Phys. **102**, 053516 (2007).